ISSSD 2019

XIX INTERNATIONAL SYMPOSIUM ON SOLID STATE DOSIMETRY

Host

CONSEJO ZACATECANO DE CIENCIA TECNOLOGÍA E INNOVACIÓN

Universidad Autónoma de Zacatecas
"Francisco García Salinas"

Proccedings
Volume I

Zacatecas, Zac. México
October 7 to 11th, 2019

ISSSD

LRSPP-based interferometric structures for biosensing.

Rafael Guzman-Cabrera[1], Carlos Giovanny Martínez-Arıas[1]
& José Rafael Guzman-Sepulveda[2].

[1] Universidad de Guanajuato, km 3.5 + 1.8 road Salamanca-Valle de Santiago Salamanca, Guanajuato, MEX, 36730

[1] Universidad de Guanajuato, km 3.5 + 1.8 road Salamanca-Valle de Santiago Salamanca, Guanajuato, MEX, 36730

[2] CREOL, The College of Optics and Photonics, University of Central Florida 4304 Scorpius St., Orlando, FL, USA

E-mail: guzmanc@ugto.mx

Abstract

In this work, we present a parametric study, by means of numerical simulations, of an integrated Mach-Zehnder interferometer, where one of the arms has been replaced by a long-range surface plasmon polariton waveguide. Our structure is designed specifically for biologically-relevant situations, where high-sensitivity sensing of refractive index in aqueous environments is critical for tracing small changes in the concentration of the suspended species. Overall, our results validate the used of the proposed structure for bio-sensing applications, based on the sensitivity obtained in our parametric study.

Keywords: LRSPP, s-bend, intensity, optical phase shift, effective mode index.

1.- INTRODUCTION

The high-sensitivity sensing of refractive index, simply referred to as bio-sensing, requires the use of structures that can be capable of discriminating between small variations of refractive index of the sample under study, from where small concentrations of solutes can be inferred. For this goal, two main approaches are commonly used.

The first approach involves the development of optical sensors that are based on extended evanescent fields. These architectures have the ability to detect small variations in the refractive index of a surrounding medium due to the strong interaction resulting from the deep penetration depth of the evanescent tails [Ionita and Kusko 2010]. An example of this is fiber-optic biosensors, which are typically tapered in order to generate the longer evanescent tails outside the optical fiber that are required for sensing [Leung *et al*., 2007]. The other approach involves using interferometric detection schemes, which are well known in optics for their large sensitivity. One typical example is the integrated Mach-Zehnder interferometer (MZI). Generally speaking, sensors based on a MZI transform the phase change induced by the change of refractive index into a modulated intensity signal which can be useful for sensing [Ionita and Kusko 2010].

A hybrid configuration that can bring together the high sensitivity of both approaches would be highly desirable: an interferometric structure with a sensing arm that can provide extended evanescent tails. In this regard, the sensitivity of those interferometric devices can be increased by using so-called Long-Range Surface Plasmon Polariton (LRSPP) waveguides [Berini 2009]. LRSPP are transverse magnetic (TM) surface waves that propagate on a thin metal slab cladded by dielectrics of similar refractive index [Berini 2009, Maier 2007]. In LRSPP-based sensors, given that the waveguide consists of a thin metal waveguide, the light propagates mostly outside the core thus allowing a strong interaction between the light and the medium surrounding the waveguide. This concept has been actually used to demonstrate all-plasmonic integrated passive optical components [Charbonneau *et al*., 2005, Charbonneau *et al*., 2006], including interferometers with dual- [Fan and Berini 2016] and triple-arm configurations [Fan *et al*., 2014, Fan and Berini 2016]. Despite their great sensitivity, one of the main drawbacks of all-plasmonic optical

devices is their inherently higher losses due to the absorption in the metallic portions of the device, which in some cases can constitute practically the entire device.

In this work, we present the design and numerical simulations of an integrated MZI sensor, where the sensing arm is a LRSPP waveguide while the rest of the device is all-dielectric and lossless. In that LRSPP waveguide, the top cladding is removed in order for the waveguide to exposed to the analyte, which plays the role of the top cladding for the waveguide. This allows for high-sensitivity sensing of small variations in the refractive index of the analyte. Specifically, our device is designed for cases where the analyte consists of aqueous media. Our numerical study was carried out using the COMSOL Multiphysics software [Fan and Berini 2016, COMSOL 2015], and considering the case of ideal interference, where the two arms of the interferometer are assumed to have balanced intensity. Overall, our results demonstrated the feasibility of using the proposed structure for bio-sensing applications, based on the sensitivity obtained in our parametric study.

2.- STRUCTURE OF THE DEVICE

In general terms, an integrated MZI structure consists of a straight waveguide (input port), which is splitted by a Y-junction into two arms, which are re-combined by another Y-junction at the end of the active sensing length into another straight waveguide (output port) [Ionita and Kusko 2010, Krupin *et al*., 2017], as shown schematically in Fig. 1(a).

In very general terms, like any other interferometer, the response of a MZI is based on the difference in the phase accumulated after propagation in the reference and the sensing arm [Fan and Berini 2016, Krupin *et al*., 2017, Lee *et al*., 2017]. This phase change, which is produced by the difference between the optical paths in the two arms, translates into a sinusoidal modulation of the light intensity at the output port. Therefore, a MZI can be used as a sensor and its response can be associated to either changes in the physical length of the arms [Lee *et al*., 2017], or changes in their optical properties (arms of equal physical length) [Ionita and Kusko 2010, Krupin *et al*., 2017], or both.

In our configuration, as shown in Fig. 1, we start from an all-dielectric integrated MZI in which the sensing arm has been replaced by a LRSPP waveguide, in order to enhance the sensing sensitivity, due to the characteristic longer evanescent tails of its supported mode, while maintaining a relatively low attenuation [Chiu *et al*., 2010].

The rest of the structure of the MZI is all-dielectric, and it consists of waveguides made of the commonly-used SU8 photoresist, which are embedded into a CYTOP host polymer matrix. Figure 1(b) shows in detail the region of the sensing arm having the LRSPP waveguide. The waveguide itself consists of a thin stripe of gold [thickness ~35nm; see Figure 1(c)]. The thickness of the LRSPP waveguide has been strategically chosen in order to balance the sensitivity and the losses [Ionita and Kusko 2010]. The top cladding of the LRSPP waveguide is removed in order to expose the waveguide to interact with the analyte i.e., basically, the analyte plays the role of the top cladding of the LRSPP. Due to the large sensitivity of the mode supported by the LRSPP waveguide to the optical symmetry of the claddings, small variations in the effective refractive index of the analyte can be detected. Figure 1(d) shows the intensity distribution of the mode supported by the LRSPP waveguide, for the case of symmetric claddings.

Cytop has been considered as a material for claddings because the biological material that is to be detected is typically in an aqueous solution form. Generally, aqueous solutions have an effective refractive index close to that of water (~ 1.33) in the dilute limit [Krupin *et al*., 2017, Krupin *et al*., 2017]. The refractive index of Cytop, at an operating length of 1550 nm is, 1.34 [Khanarian and Celanese 2001, Leosson and Agnarsson 2012]. In this way, the optical symmetry around the metal waveguide can be mostly preserved when using Cytop as a cladding. We have selected the commonly-used polymer SU8 to be the material of the core of the dielectric waveguides. The refractive index of the SU8 at the operation wavelength (1550nm) is significantly larger than that of Cytop [Ionita and Kusko 2010], as shown in Table 1, which allows ensuring total internal reflection (TIR) and a good confinement.

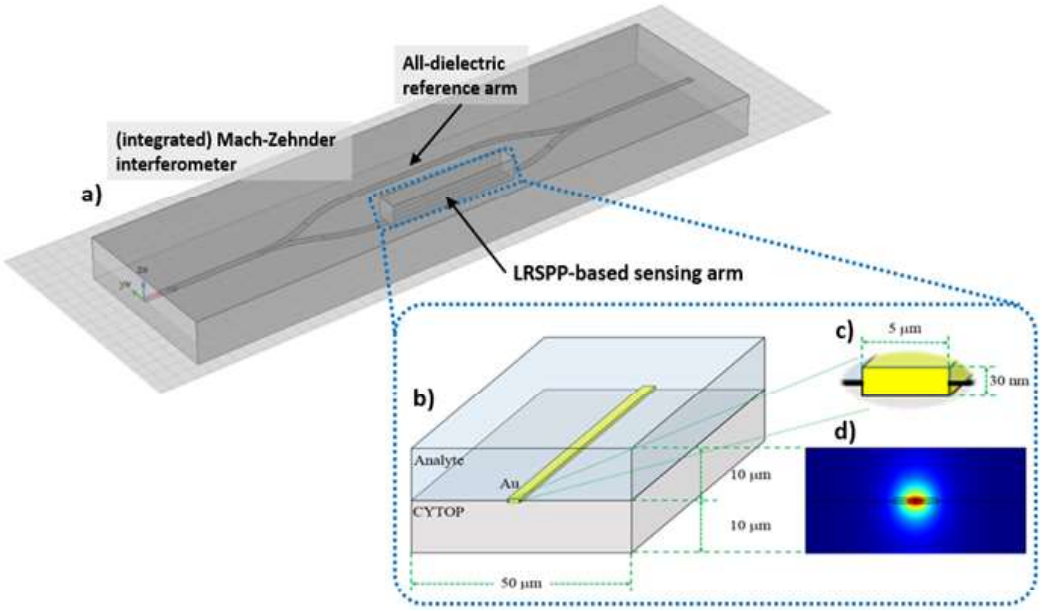

Figure 1.- (a) Schematic of the simulated device, consisting of a LRSPP waveguide incorporated into the sensing arm of an integrated MZI. (b) Zoom-in in to the sensing region. The top cladding of the LRSPP waveguide is removed in order to expose the waveguide to interact with the analyte. (c) Dimensions of the LRSPP waveguide. (d) intensity distribution of the optical mode supported by the LRSPP waveguide.

Table 1.- Table with the relevant optical characteristics (at an operating free-space wavelength of 1550nm) of the materials used in our simulations.

Materials	Refractive index (n)	Extintion Coefficient (k)	R. Permittivity (εr)
SU8	1.575	-	-
Cytop	1.34	-	-
Gold (Au)	0.55	11.4912	-132 + j 12.65

3.- RESULTS

As mentioned before, the interference between the signal in the reference arm and the sensing arm is practically modulated by the difference in the optical path between the two arms. Given that in our configuration both arms have the same physical length, L, the phase difference is determined only by the difference in the effective refractive index of the propagating optical modes [Ionita and Kusko 2010, Krupin *et al*., 2017]:

$$\Delta\varphi = \frac{2\pi L}{\lambda}\left(n_{eff,r} - n_{eff,s}\right) \quad (1)$$

where $n_{eff,r}$ is the effective refractive index of the optical mode supported by the dielectric waveguide in the reference arm, and $n_{eff,s}$ is the real part of the effective refractive index of the optical mode supported by the plasmonic waveguide in the sensing arm.

According to Ref. [Fan and Berini 2016], the characteristic propagation length, L_p, of an LRSPP waveguide with a thickness of ~35nm can be slightly longer than 2mm. At the same time, it is desired that the active sensing length is as long as possible. Therefore, throughout this work we will use a MZI whose arms have length of 2mm, which allows maximizing the interaction distance for sensing without inducing significant losses. This parameter will be kept fixed throughout our simulations. Just for reference, in Fig. 2 we show the intensity distribution of the mode in the reference arm, which is supported by a dielectric waveguide of SU8 embedded in a matrix of Cytop, and has $n_{eff,r}$ = 1.3397. It is important to highlight the symmetry of the field distribution in this waveguide due to the top and bottom cladding have the same optical characteristics. As it will be shown later, this symmetry is significantly perturbed, if not completely broken, for the case of the plasmonic waveguide in the reference arm, where one of the claddings if kept fixed and the other one is the sample under test.

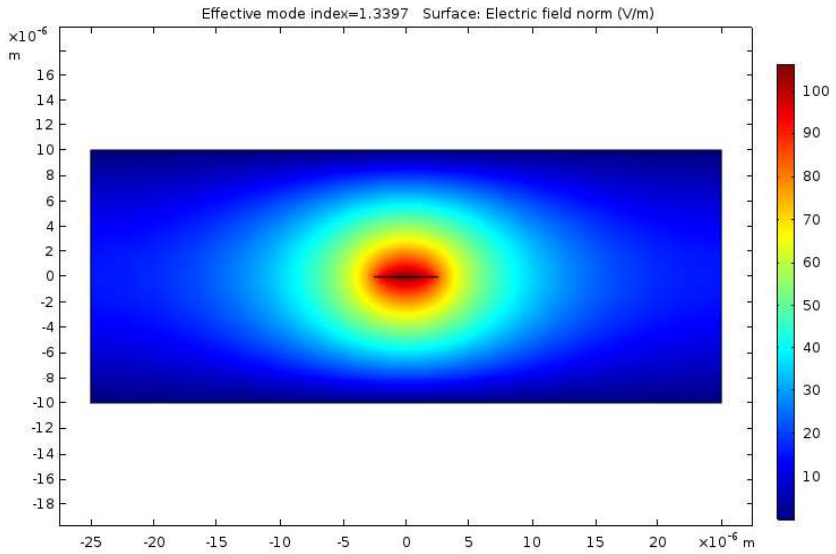

Figure 2.- Intensity distribution of the optical mode supported by reference arm, which consists of an all-dielectric waveguide whose core is made of SU-8 and it is embedded into a matrix of Cytop polymer.

Finally, at the output port of the integrated MZI waveguide, the intensity resulting from the combination of the electromagnetic waves that propagated through the arms of the MZI can be detected. The output intensity is characterized by being changed by the phase difference between the reference arm and the sensing arm [Ionita and Kusko 2010]. The normalized output intensity can be represented simply as:

$$I = \frac{1}{2}\left(1 + \cos \Delta\varphi\right) \tag{2}$$

Eq. (2) represents the case of ideal interference, where the two arms of the interferometer are assumed to have balanced intensity thus providing an interference signal with the largest possible contrast i.e., the output intensity ranges from 0 to 1; in other words, the output signal has unitary visibility.

As mentioned, we aim at detecting small variations for aqueous solutions. Therefore, we explored a refractive index range of the top cladding, which is the same as the analyte $n_{analyte}$, from 1.320 to 1.355, in steps of $1x10^{-4}$.

Strictly speaking, changes in $n_{analyte}$ affect the complex effective index of the LRSPP, $n_{LRSPP} = n_{eff} + k_{eff}$ [Martinez-Arias *et al.*, 2018]. In fact, based on this idea, the straight LRSPP waveguide alone can be actually used as a sensor that is based on the attenuation $\alpha = k_{eff}k_0$ produced by the change in the refractive index in the top cladding [Krupin *et al.*, 2017].

Nevertheless, by incorporating a LRSPP straight waveguide into a MZI configuration, our interest focuses mainly on the real part of the effective refractive index of the plasmon mode (this is what induces the phase difference in the interference), which turns out to be the effective refractive index of the sensing arm $n_{eff} = n_{eff,s}$. Therefore, our simulation strategy consists basically on the numerical calculation of n_{effs} as function of $n_{analyte}$; then, we calculated the corresponding phase difference, using Eq. (1); and, finally, we obtained the modulated intensity at the output of the MZI, using Eq. (2).

Fig. 3(a) shows how n_{effs} changes with $n_{analyte}$. The blue points are particular cases for which the intensity distribution was analyzed in more detail, as it will be shown later. The inset shows the difference with respect to the reference arm, $\Delta n_{eff} = n_{eff,r} - n_{eff,s}$.

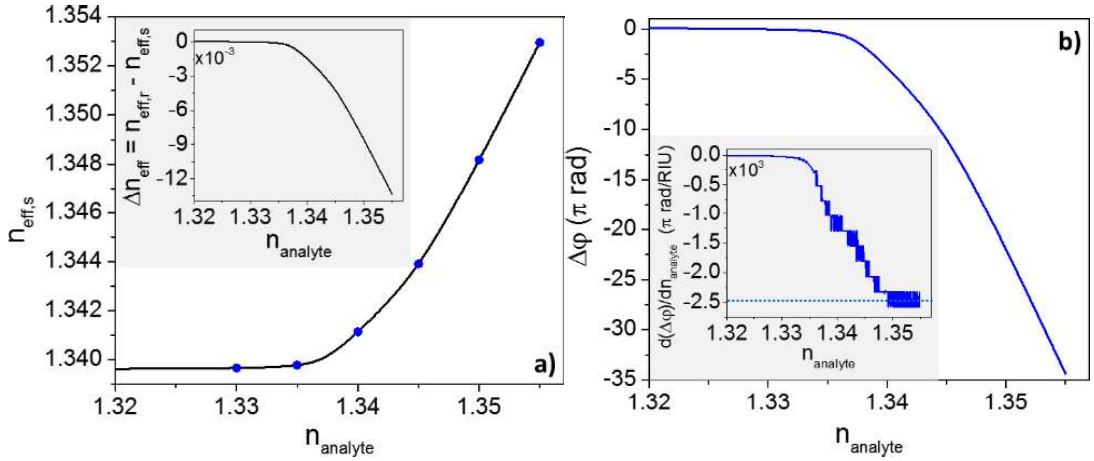

Figure 3.- (a) Effective refractive index of the mode in the LRSPP waveguide, n_{effs}, as a function of the refractive index of the analyte, $n_{analyte}$. The inset shows the difference with respect to the reference arms, $\Delta n_{eff} = n_{eff,r} - n_{eff,s}$. The blue points in the main plot represent particular cases for which the intensity distribution was analyzed in more detail (see Fig. 4). (b) the corresponding phase difference, $\Delta\varphi$, calculated using Eq. (1), for an operating wavelength of 1.55μm and a length of the arms in the MZI of L = 2mm. The inset shows the derivative (local slope) of the curve in the main plot, which is a direct measure of the sensitivity of the device. From this plot, a huge sensitivity can be expected due to the large phase difference induced with a small change in $n_{analyte}$ (see text for details).

Fig. 3(b) shows the corresponding phase difference, $\Delta\varphi$, calculated using Eq. (1), for an operating wavelength of 1.55μm and a length of the arms in the MZI of L = 2mm. The inset shows the derivative of the curve in the main plot, which is a direct measure of the sensitivity of the device. This is precisely the hallmark of the combination of an interferometer and a plasmonic structure with long evanescent tails – it's extremely large response.

In fact, it has been recently demonstrated that such characteristic can be advantageous for the construction of highly integrated devices where a massive phase modulation can be achieved [Fuentes- Fuentes *et al*., 2019, Torres-Cisneros *et al*., 2019].

In our particular case, the maximum change in the phase difference that can be achieved is of about $2.5\text{x}10^{3}$ (πrad)/RIU (see Fig. 3(b)); this means that a small change $n_{analyte}$ of only $4\text{x}10^{-4}$ will be sufficient to induce a change in the phase difference of π rad, which would cover basically the whole dynamic range of the interferometer (see Eq. (2)).

Fig. 4 shows the intensity distribution of the mode supported by the LRSPP waveguide, for the values of $n_{analyte}$ indicated in Fig. 3(a). It can be seen that for cases when $n_{Analyte}<n_{Cytop}$ most of the field is at the bottom cladding, outside the waveguide (Fig. 4(a)-(b)). As the difference between the refractive indices of the bottom and top claddings decreases, the intensity distribution is becoming more symmetric and most of the field is around the core, as shown in Figure 4(c). Finally, when $n_{Analyte}>n_{Cytop}$ most of the field is again outside the waveguide, this time displaced towards the detection window (top cladding; Fig. 4(d)-(f)).

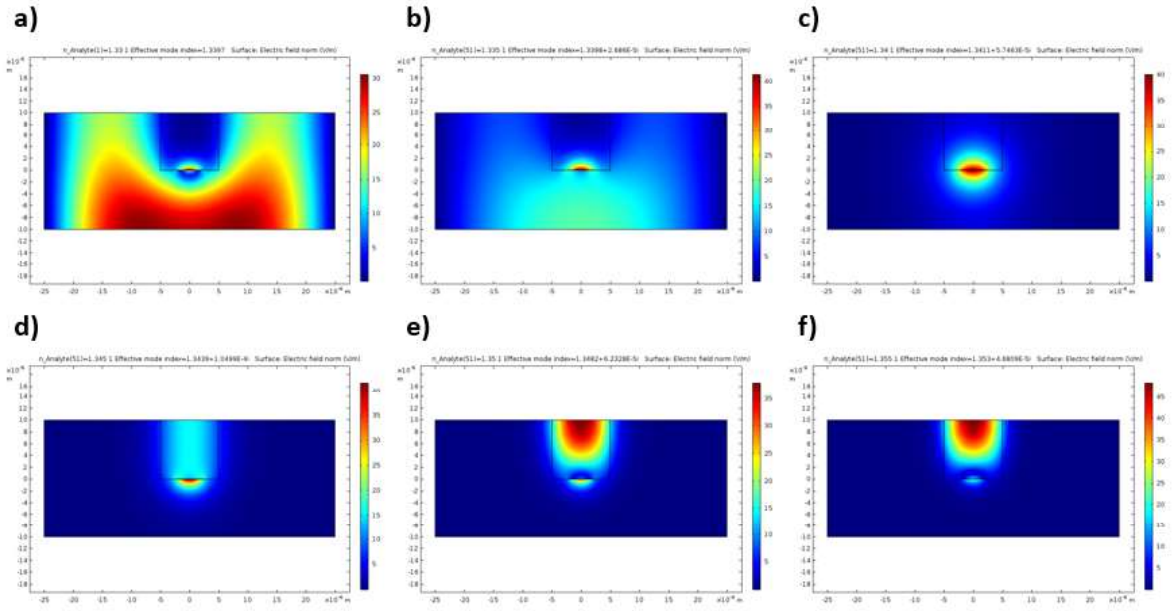

Figure 4.- Intensity distribution of the optical mode supported by the LRSPP waveguide when the refractive index of the analyte $n_{Analyte}$ is a) 1.330, b) 1.335, c) 1.340, d) 1.345, e) 1.350 and f) 1.355, respectively.

Fig. 5(a) shows the normalized output of the MZI, calculated using Eq. (2), for the refractive index range of interest. Fig. 5(b) shows the local slope of the intensity curve in panel (a), in the linear portion of the curve i.e., at the point of half-intensity. Together with the sensitivity, in the secondary axis of Fig. 5(b), we plot the dynamic range for an unambiguous measurement of refractive index i.e., the separation distance between adjacent peaks in the intensity curve.

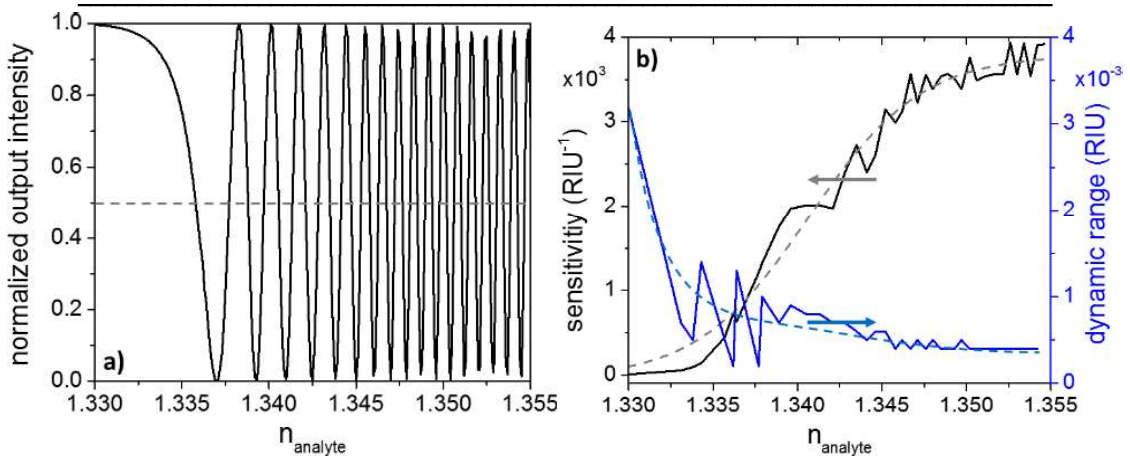

Figure 5.- (a) Normalized output intensity of the MZI, calculated using Eq. (2). (b) the corresponding sensitivity (at the point of half-intensity).

Overall, Fig. 5(b) illustrates the compromise for refractive index sensing between the dynamic range of the measurement and the sensitivity at which the measurement can be performed: the larger the sensitivity the smaller the dynamic range.

In other words, these curves verify that a wide range of refractive index can be covered only with a low sensitivity; while, on the other hand, if the measurement is performed in a small range of refractive index, the benefit of a larger sensitivity can be exploited for the measurement. In our particular case, the largest sensitivity that can be achieved is larger than $3x10^3$ RIU^{-1}, which is suitable for biosensing.

It is important to note that the sensing sensitivity is dictated by the phase difference that can be induced between the two arms and it does not depend on their actual intensity. However, it is desirable that the two arms of the interferometer have balanced intensity in order to provide the maximum possible quality of the signal measured i.e., to achieve unitary visibility, as in the ideal case (Fig. 5(a)).

4.- FINAL REMARKS

We presented a parametric study of an integrated refractive index sensing platform consisting of a Mach-Zehnder interferometer, where one of the arms was replaced by a long-range surface plasmon polariton waveguide. In this way, we combine the high sensitivity of the two more common approaches used for biosensing: an interferometric

sensing platform with a sensing arm that can provide extended evanescent tails for stronger interaction with the device's surroundings.

Our structure is designed specifically for biologically-relevant situations, where high-sensitivity sensing of refractive index in aqueous environments. Overall, we demonstrated that a sensitivity larger than $3x10^3$ RIU^{-1} can be achieved which is suitable for biosensing applications.

Finally, in the present work, we addressed the case of ideal interference, where the two arms of the interferometer were assumed to have balanced intensity. Future work will consist on the geometrical optimization of the device, especially the Y-junctions, in order to actually achieve this.

REFERENCES

Berini, P. (2009). *Long-range surface plasmon polaritons*. Advances in optics and photonics, 1(3), 484-588.

Charbonneau, R., Lahoud, N., Mattiussi, G., Berini, P. (2005). *Demonstration of integrated optics elements based on long-ranging surface plasmon polaritons*. Optics Express, 13(3), 977-984.

Charbonneau, R., Scales, C., Breukelaar, I., Fafard, S., Lahoud, N., Mattiussi, G., Berini, P. (2006). *Passive integrated optics elements based on long-range surface plasmon polaritons*. Journal of Lightwave Technology, 24(1), 477-494.

Chiu C., Lisicka-Skrzek E. Tait R. N., Berini P. (2010). *Fabrication of surface plasmon waveguides and devices in Cytop with integrated microfluidic channels*. J. Vac. Sci. Technol. B 28(4).

COMSOL Multiphysics (2015): Application Library Manual. Wave optics Module. v5.2.

Fan H., Berini P. (2016): Bulk sensing using a long-range surface-plasmon dual-output Mach–Zehnder interferometer. Journal of Lightwave Technology, 34(11), 2631-2638. doi: 10.1109/JLT.2016.2543138.

Fan H., Charbonneau, R., Berini P. (2014): Long-range surface plasmon triple-output Mach-Zehnder interferometers. Optics express, 22(4), 4006-4020. doi: 10.1364/OE.22.004006.

Fan, H., & Berini, P. (2016): Bulk sensing using a long-range surface-plasmon triple-output Mach–Zehnder interferometer. JOSA B, 33(6), 1068-1074. doi: 10.1364/JOSAB.33.001068.

Fuentes-Fuentes, M. A., May-Arrioja, D. A., Guzman-Sepulveda, J. R., Arteaga-Sierra, F., Torres-Cisneros, M., Likamwa, P. L., Sánchez-Mondragón, J. J. (2019): Suspended LRSPP for the development of highly integrated active plasmonic devices. Optics express, 27(6), 8858-8870. doi: 10.1364/OE.27.008858.

Ionita M. R., Kusko M. (2010): Desıgn and Sımulatıon of an Integrated Mach-Zehnder Interferometer Sensor. CAS 2010 Proceedings (International Semiconductor Conference), 529–532 doi: 10.1109/SMICND.2010.5650448.

Khanarian, G. and Celanese, H.: Optical properties of cyclic olefin copolymers. Opt. Eng. (2001), doi: 10.1117/1.1369411.

Krupin O., Khodami M., Fan M., Wong W. R., Mahamd Adikan F. R., Berini P. (2017): Biosensing using long-range surface plasmon waveguides. Proc. of SPIE Vol. 10242, 1024203, Physics and Simulations III, doi: 10.1117/12.2268976.

Krupin, O., Wong, W. R., Mahamd Adikan, F. R. and Berini, P (2017): Detection of Small Molecules Using Long-Range Surface Plasmon Polariton Waveguides. IEEE J. Sel. Top. Quantum Electron. 23(2),doi: 10.1109/JSTQE.2016.2611593.

Lee D. E., Lee Y., J. Shin E., Kwon S. H. (2017): Mach-Zehnder Interferometer Refractive Index Sensor Based on a Plasmonic Channel Waveguide. Sensors, 17, 2584; doi: 10.3390/s17112584.

Leosson, K. and Agnarsson, B.: Integrated biophotonics with CYTOP. Micromachines 3(1), 114–125 (2012), doi:10.3390/mi3010114.

Leung A., Shankar P. M., Mutharasan R. (2007): A review of fiber-optic biosensors. Sensors and Actuators B 125 688–703, doi: 10.1016/j.snb.2007.03.010.

Maier, S. A. (2007): Plasmonics: fundamentals and applications. Springer Science & Business Media.

Martínez-Arias C. G., Escobar M. A., Guzman-Sepulveda J. R., Torres-Cisneros M., Guzman-Cabrera R. (2018): Biosensing using long-range surface plasmon structures. Proc. SPIE 10728, Biosensing and Nanomedicine XI, doi: 10.1117/12.2320281.

Torres-Cisneros, M., Fuentes-Fuentes, M. A., May-Arrioja, D. A., Guzman-Sepulveda, J. R., LiKamWa, P. L., Sánchez-Mondragón, J. J. (2019): Novel Structures' Configurations for Long-Range Surface Plasmon-Polaritron. Computación y Sistemas, 23(1), 121. doi: 10.13053/CyS-23-1-3172.